# BIOCHEMICAL PROFILES OF MEMBRANES FROM X-RAY AND NEUTRON DIFFRACTION

LEON MCCAUGHAN AND S. KRIMM
*Biophysics Research Division, The University of Michigan, Ann Arbor, Michigan 48109*

ABSTRACT X-ray and neutron diffraction methods provide some information about the distribution of mass in biological membranes and lipid-water systems. Scattering density profiles obtained from these systems, however, usually are not directly interpretable in terms of the relative amounts of chemical constituents (e.g., lipid, protein, and water) as a function of position in the membrane. We demonstrate here that the combined use of x-ray and neutron-scattering profiles, together with information on the total amounts of each of the major membrane components, are sufficient to calculate unambiguously the volume fractions of these components at well-defined regions of the lamellar unit. Three cases are considered: a calculated model membrane pair, dipalmitoylphosphatidylcholine-water multilayers, and rabbit sciatic nerve myelin. For the model system, we discuss the limitations imposed by finite resolution in the diffraction patterns. For the lipid-water multilayers, we calculate water volume fractions in the hydrocarbon tail, lipid headgroup, and interlamellar regions; estimates of these values by various methods are in good agreement with our results. For the nerve myelin, we predict new results for the distribution of protein through the membrane.

## INTRODUCTION

The past two decades have seen the steady development and refinement of experimental and theoretical diffraction methods applied to biological membrane samples with one-dimensional periodicity. Electron density profiles have been determined from x-ray diffraction patterns for a variety of biological membranes, including myelin (1–3), rod outer segments (4–6), and the human erythrocyte membrane (7–9). More recently, neutron-scattering profiles have also been obtained for these systems (9–13).

Neither approach, taken separately, is capable of describing quantitatively the distribution of chemical constituents of the membrane as a function of position across the lamellar profile. It is this information that is needed to develop correlations between the biological functioning of the membrane and its structure. However, because the different biochemical components (lipid, protein, and water) have different relative x-ray and neutron-scattering amplitudes, the two profiles contain independent information on the relative distribution of these components. It should, therefore, be possible to obtain a "biochemical profile" of the membrane from an analysis of the two scattering density profiles.

We have formulated the theory for unambiguously relating (*a*) the magnitudes in an x-ray and two neutron-scattering density profiles (the latter at two $H_2O/D_2O$ ratios), (*b*) the known scattering amplitudes of the various components, and (*c*) total composition data on the system, to the volume fractions of the components in well-defined regions of the lamellar unit. We have applied this theory to a model system, to investigate the limitations of the method, to a lipid bilayer system, where the results agree with estimates made by others, and to myelin profiles, for which reasonable predictions can be made.

## THEORY

Scattering density profiles are density distributions perpendicular to the plane of the membrane and averaged over that plane. The mathematical representation of diffraction, which relates a diffraction pattern (scattering intensity as a function of scattering angle) to its scattering density distribution, is the same for both coherently scattered x-ray photons and for neutrons. The scattering amplitude is given by

$$F(h/d) = \sum_j f_j \exp(2\pi i x_j h/d), \qquad (1)$$

and the scattering density distribution by

$$\rho(x) = \frac{1}{d}\sum_h F(h/d) \exp(-2\pi i x h/d), \qquad (2)$$

where $h$ is the order of the reflection, $d$ is the lamellar periodicity, and $f_j$ is the coherent scattering amplitude (a function of scattering angle for the x-ray case and a constant for the neutron case) of the $j$th atom located at $x_j$.

X-ray and neutron coherent scattering amplitudes of the elements bear no linear relationship to one another. X-ray scattering amplitudes are proportional to the atomic number, $Z$. The x-ray scattering density is therefore proportional to the electron density in the scattering

system. No equivalent relationship exists for the neutron-scattering density of an element (14). The two types of scattering profiles (x ray and neutron) therefore provide independent information about the same mass distribution in the scattering object.

The information available from x-ray or neutron-scattering density profiles is, however, incomplete. Because the diffraction pattern is almost always collected in arbitrary intensity units, and its forward scattering intensity (coincident with the undiffracted beam) is not measurable, the pattern and its scattering density profile are known only to within additive and multiplicative (scaling) constants. That is, if $\zeta(x)$ and $\eta(x)$ are the calculated relative x-ray and neutron-scattering density profiles, respectively, and $\rho(x)$ and $\sigma(x)$ are their absolute scattering density counterparts, then

$$\rho(x) = A\zeta(x) + a \tag{3}$$

and

$$\sigma(x) = B\eta(x) + b, \tag{4}$$

where $A$ and $B$ are scaling factors and $a$ and $b$ determine the absolute values of $\rho$ and $\sigma$.

Difference ratios between three points on the absolute profiles ($\rho$ or $\sigma$) can, however, be directly related to those on the relative profiles ($\zeta$ or $\eta$). For example, for the x-ray scattering density profile,

$$R_0 \equiv \frac{\zeta(x_i) - \zeta(x_j)}{\zeta(x_k) - \zeta(x_j)} = \frac{\rho(x_i) - \rho(x_j)}{\rho(x_k) - \rho(x_j)}. \tag{5}$$

Typically, two very different neutron-scattering density profiles, $\sigma_1(x)$ and $\sigma_2(x)$, can be recorded from one membrane or lipid bilayer specimen if its aqueous component is equilibrated with two different ratios of $H_2O/D_2O$. (As can be seen from Table I and Figs. 1–3, this change in the scattering densities of components with exchangeable hydrogens can be dramatic.) Given that $D_2O$ is chemically identical to $H_2O$, the change in the scattering density of any component containing exchangeable hydrogens will be directly proportional to the change in concentration ratio of $H_2O/D_2O$ at $x_i$. Consequently, scattering profiles at two different $H_2O/D_2O$ ratios completely determine profiles at all ratios: only two linearly independent relationships can therefore be constructed for one-dimensional (lamellar) profiles of a membrane system with exchangeable hydrogens (cf. reference 16 for other consequences). We there-

TABLE I
COHERENT SCATTERING DENSITIES CALCULATED FOR MEMBRANE COMPONENTS*

| Component | X-ray‡ ($\rho^e$) | Neutron§ ($\sigma^e$) | |
|---|---|---|---|
| | | 100% $H_2O$ | 100% $D_2O$ |
| Water | 9.40 | −0.60 | 6.30 |
| Protein‖ | 12.00 | 1.90 | 3.30 |
| Phospholipid | | | |
| Phosphorylcholine | 13.00 | 1.10 | 1.10 |
| Methylene chains | 8.10 | −0.31 | −0.31 |
| Methyl groups | 4.62 | −0.85 | −0.85 |
| Myelin headgroups¶ | 13.00 | 0.80 | 1.60 |
| Total lipid | | | |
| DPC | — | 0.19 | 0.19 |
| Myelin (average)** | — | 0.50 | 0.70 |

*The scattering density is taken to be the sum of the scattering magnitudes of the atoms divided by the volume of the group involved.

‡In units of $10^{14}$ cm/Å$^3$. To convert to electrons/Å$^3$, divide by $2.8 \times 10^{-13}$.

§In units of $10^{14}$ cm/Å$^3$. Neutron-scattering densities at intermediate $H_2O/D_2O$ ratios are obtained by linear interpolation.

‖20% of the hydrogens are assumed to be exchangeable (10).

¶The myelin headgroup is represented by phosphorylcholine. (To our knowledge, the lipid composition of rabbit sciatic nerve myelin has not been determined.) The phospholipid distribution of bovine spinal root myelin (15) was used to calculate the effect of exchangeable hydrogens on the neutron-scattering densities of myelin headgroups, viz., 11% choline-, 13% ethanolamine-, 7% serine-glycerophosphatides; 14% sphingomyelin; 11% cerebrosides; and 44% cholesterol on a mole-percent basis.

**Includes 40 mol/100 mol cholesterol.

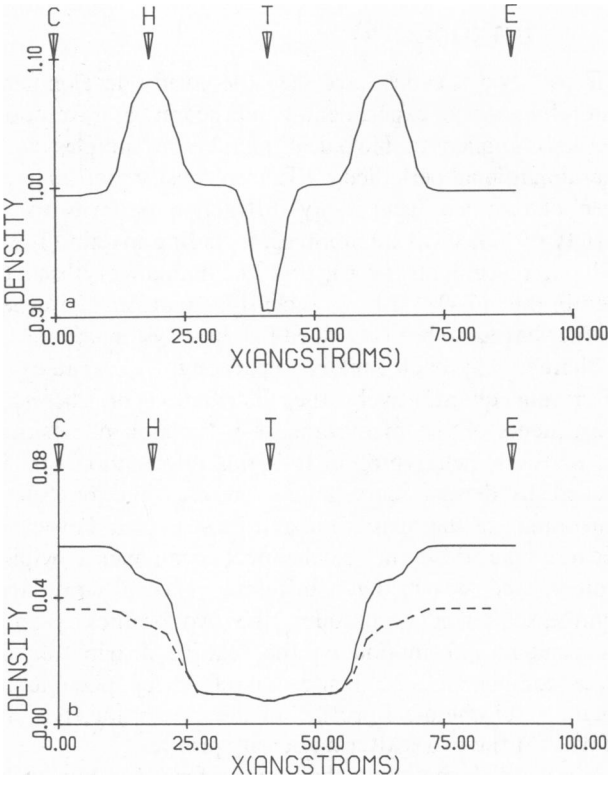


FIGURE 1 Model membrane-scattering density profiles. Model profiles are patterned approximately after the myelin membrane pair, with a 180-Å unit cell. Scattering densities in (cm/Å$^3$) $\times 10^{13}$ are step-profiles smoothed by convolution with a gaussian function of 5.7 Å full width at $e^{-1}$. (*a*) X-ray scattering density distribution, $\rho$ $(x)$; (*b*) neutron-scattering density distributions at 65% $D_2O$ (---) $[\sigma_1(x)]$ and 100% $D_2O$ (—) $[\sigma_2(x)]$. The points C (cytoplasmic), H (headgroup), and T (hydrocarbon tail) used for calculation of the difference ratios are shown.

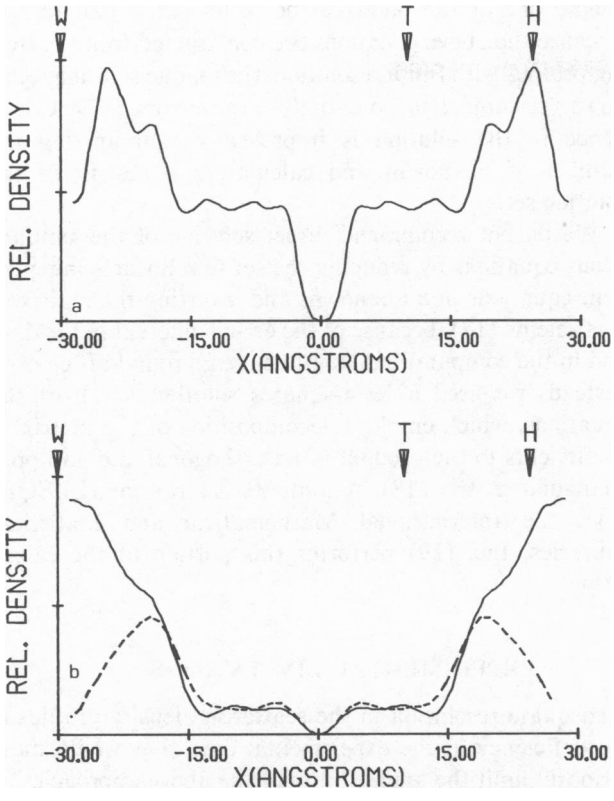


FIGURE 2 Scattering density profiles of L-$\alpha$-DPC-water multilayers at 57.7 Å lamellar periodicity. (*a*) X-ray profile redrawn from Torbet and Wilkins (21). (*b*) Neutron profiles at 100% $D_2O$ (—) and 100% $H_2O$ (- - - -) redrawn from Worcester (24). Difference ratios were calculated using the profile values at W (aqueous) and H (headgroup). The third value, the methylene chains of the tail (T), is represented by the average over $5 \leq |x| \leq 15$ Å.

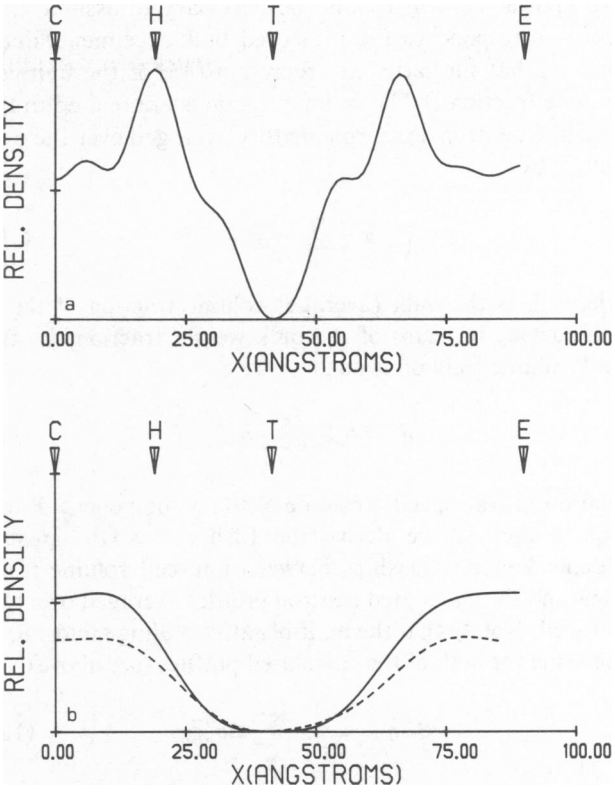


FIGURE 3 Scattering density profiles of rabbit sciatic nerve myelin in Ringer's solution. Lamellar periodicity is 180 Å. The points C (cytoplasmic), H (headgroup), T (hydrocarbon tail), and E (extracellular) are defined by the x-ray profile. (*a*) X-ray profile resynthesized from 18 orders of diffraction (3); (*b*) neutron profiles of myelin in 100% $D_2O$ (—) calculated from 7 orders of diffraction (10) and in 65% $D_2O$ (- - - -) calculated from 6 orders.

fore can define two independent difference ratios

$$R_{1,2} \equiv \frac{\eta_{1,2}(x_i) - \eta_{1,2}(x_j)}{\eta_{1,2}(x_k) - \eta_{1,2}(x_j)} = \frac{\sigma_{1,2}(x_i) - \sigma_{1,2}(x_j)}{\sigma_{1,2}(x_k) - \sigma_{1,2}(x_j)}. \quad (6)$$

Because exchangeable hydrogens of the diffracting specimen are stoichiometrically replaced by deuterons, the remainder of the specimen being left unchanged, the two scattering density profiles can be correctly scaled to one another (taking into account absorption corrections). The constant $B$ in Eq. 4 is therefore the same for both neutron profiles, $\sigma_1(x)$ and $\sigma_2(x)$. A fourth equation can then be constructed by considering a ratio of differences between two neutron-scattering profiles:

$$R_3 \equiv \frac{\Delta\eta(x_i) - \Delta\eta(x_j)}{\Delta\eta(x_k) - \Delta\eta(x_j)} = \frac{\Delta\sigma(x_i) - \Delta\sigma(x_j)}{\Delta\sigma(x_k) - \Delta\sigma(x_j)}, \quad (7)$$

where $\Delta\sigma(x) \equiv \sigma_2(x) - \sigma_1(x)$ and $\Delta\eta(x) \equiv \eta_2(x) - \eta_1(x)$.

If the three points $x_i$, $x_j$, and $x_k$ on the unit-cell scattering density profiles of a membrane system are sufficiently well defined, the above ratios can be described in terms of the fractional amount of each constituent present, which we assume to be lipid, protein, or water. This is possible since

$$\rho(x_m) = \sum_\alpha \rho_\alpha^0 g_\alpha(x_m) \quad (8)$$

and

$$\sigma(x_m) = \sum_\alpha \sigma_\alpha^0 g_\alpha(x_m) \quad (9)$$

where $m = i, j, k$, and the value of $\sigma_\alpha^0$ is a function of the $H_2O/D_2O$ ratio of $\sigma(x)$ (see Table I‡). Here $g_\alpha(x_m)$ represents the volume fraction of the $\alpha$ chemical constituent present in the unit cell at $x_m$ (i.e., $\Sigma g_\alpha = 1$), and $\rho_\alpha^0$ and $\sigma_\alpha^0$ are known values of the x-ray and neutron-scattering densities of the $\alpha$ component, respectively. We give such values in Table I. Substitution of Eqs. 8 and 9 into Eqs. 5–7 produces four expressions in terms of the volume fractions of the membrane components at three points on the profile.

Two additional relationships for the lamellar unit can be established if the volume fractions of its major components (for example, of lipid and water in lipid-water multilayers)

are known. (It will usually be necessary to assume that these correspond to the measured bulk specimen values; that is, that the latter are representative of the unit-cell volume fractions.) The volume fractions are related to the absolute neutron-scattering density averaged over the unit cell, $\bar{\sigma}$, by

$$\bar{\sigma} = \sum_{\alpha} \sigma_{\alpha}^{0} \bar{g}_{\alpha}, \tag{10}$$

where $\bar{g}_{\alpha}$ is the bulk (average) volume fraction of the $\alpha$ component. In terms of the bulk weight fraction, $\bar{h}_{\alpha}$, the bulk volume fraction is just

$$\bar{g}_{\alpha} = \bar{h}_{\alpha} \bar{v}_{\alpha} \Big/ \sum_{\alpha} \bar{h}_{\alpha} \bar{v}_{\alpha}, \tag{11}$$

where $\bar{v}_{\alpha}$ is the specific volume of the $\alpha$ component. From Eqs. 4 and 10 we derive the fifth and sixth linearly independent relationships between unit-cell volume fractions and the calculated neutron profiles averaged over the unit cell. Noting that the multiplicative scaling factor, $B$, is the same for both of the calculated profiles (see above),

$$B\Delta\bar{\eta} + \Delta b = \sum_{\alpha} \Delta\sigma_{\alpha}^{0} \bar{g}_{\alpha} \tag{12}$$

where $\Delta\sigma_{\alpha}^{0} \equiv \sigma_{\alpha,2}^{0} - \sigma_{\alpha,1}^{0}$ of the $\alpha$ membrane component, $\Delta b \equiv b_2 - b_1$, and $\Delta\bar{\eta} \equiv \bar{\eta}_2 - \bar{\eta}_1$. Letting the subscript "2" represent the neutron scattering profile with the larger $D_2O$ content, the sixth equation, using Eqs. 4 and 10, is

$$B\bar{\eta}_2 + b_2 = \sum_{\alpha} \sigma_{\alpha,2}^{0} \bar{g}_{\alpha}. \tag{13}$$

The terms $\Delta b$ and $b_2$ in Eqs. 12 and 13 can be expressed as a function of the component volume fractions at one of the three points ($m = i, j, k$) on the neutron-scattering profiles, using Eqs. 4 and 9:

$$B[\Delta\bar{\eta} - \Delta\eta(x_m)] + \sum_{\alpha} \Delta\sigma_{\alpha}^{0} g_{\alpha}(x_m) = \sum_{\alpha} \Delta\sigma_{\alpha}^{0} \bar{g}_{\alpha} \tag{14}$$

$$B(\bar{\eta}_2 - \eta_2(x_m)) + \sum_{\alpha} \sigma_{\alpha,2}^{0} g_{\alpha}(x_m) = \sum_{\alpha} \sigma_{\alpha,2}^{0} \bar{g}_{\alpha} \tag{15}$$

Eqs. 5–7, 14, and 15 will therefore produce six independent equations written in terms of the unit-cell volume fractions at three points along the profile and the scaling constant $B$.

In general, up to five volume fractions, $g_{\alpha}(x_m)$ plus the scaling constant $B$, are uniquely specified by the six inhomogeneous independent equations. Three additional volume fractions, one at each of the three points of analysis on the profiles, are calculable from $\Sigma_{\alpha=1}^{3} g_{\alpha}(x_m) = 1$. Although nine volume fractions are generally required (lipid, protein, and water at three points), the system is in fact completely specified by eight fractions since we choose one of the points to be in an extra-lipid region. Because the above equations are constructed from scattering profiles with finite resolution, the unique solution set is, however, subject to potentially large errors (17). Confidence in the solution is improved by minimizing the number of unknowns and calculating a best-fit of the solution set.

We do not recommend direct solution of the simultaneous equations by reducing the set to $n$ linearly independent equations in $n$ unknowns and inverting the matrix of coefficients (17), because of the errors inherent in the data and in the computational methods (e.g., round-off errors). Instead, we used a least-squares solution to all of the equations, which employs decomposition of the matrix of coefficients to the product of an orthogonal and an upper triangular matrix (18). A computer subroutine (LLSQF) from the International Mathematical and Statistical Libraries, Inc. (19) performs this portion of the calculation.

## EXPERIMENTAL LIMITATIONS

Inadequate resolution in the scattering density profiles is the deficiency in the experimental data that would most seriously limit the applicability of the above approach. To evaluate the effect of limited resolution on the accuracy of the least-squares solutions, calculations were performed on a lattice of model membrane pairs. Each model membrane of the centrosymmetric pair is composed of six regions: the cytoplasmic (C) region, $0 \leq x < 15$ Å, and the extracellular (E) region, $69 < x \leq 90$ Å, each containing a water volume fraction $g_w$(C,E) = 0.77, the remaining volume fraction being protein; two headgroup (H) regions, $15 \leq x < 24$ Å and $60 < x \leq 69$ Å, with water fractions $g_w$(H) = 0.50, protein fractions $g_p$(H) = 0.34, and the remaining 16% of the volumes being occupied by phosphorylcholine; and the hydrocarbon region, $24 \leq x \leq 60$ Å, which is further divided into a 5-Å central core ($40 \leq x \leq 45$ Å) containing the terminal methyl groups of the phospholipid fatty acid tails (T region), the remaining volume consisting of methylene chains. The hydrocarbon region (including the central tail [T] region) contains 56% protein, which is inaccessible to the aqueous milieu (precluding H → D exchange), and 44% lipid.

X-ray and neutron-scattering densities for the model were calculated from Eqs. 8 and 9, using the values taken from Table I for the component's scattering densities ($\rho_{\alpha}^{0}$ and $\sigma_{\alpha}^{0}$). To avoid artifacts from the discontinuities in the model (i.e., Gibbs' phenomenon), the step profile was smoothed by convolving it with a gaussian function of 5.7 Å full width at $e^{-1}$ before resynthesis (see below). The smoothed x-ray scattering density profile of the model membrane pair is shown in Fig. 1*a* and its two corresponding neutron-scattering density profiles in Fig. 1*b*.

The difference ratios were calculated from Eqs. 5–7 using the scattering densities at the cytoplasmic ($x_i$),

hydrocarbon tail ($x_j$), and the phospholipid headgroup ($x_k$) regions. The scattering density in the cytoplasmic region is taken as the average of the profile over $0 \leq x \leq 10$ Å. As would be done with experimental data, phospholipid headgroup and tail regions are operationally defined by the peak ($x \simeq 19$ Å) and trough ($x \simeq 42$ Å), respectively, in the x-ray scattering density profile. The center of the hydrocarbon tail region ($x_j$) was arbitrarily chosen for $x_m$ in Eqs. 14 and 15. (This practice will be followed for subsequent calculations.) Note that, since $\eta_{1,2}(x)$ is arbitrary with additive and multiplicative constants, any convenient linear scale may be chosen to measure $\eta(x)$ from Fig. 1*b*.

The "observed" scattering density profiles (one x-ray and two neutron density profiles at different $H_2O/D_2O$ ratios) were then resynthesized at different resolutions from the set of structure factors calculated from the Fourier transform of the model membrane pair (sampled at $h/d$, $d = 180$ Å, $h = 1,2 \ldots$; see Eq. 2). Resolution of a reconstructed profile is nominally defined by a "resolution value," $d/N$, where $d$ is the lattice repeat period and $N$ is the number of structure factors used in the synthesis.

Neutron diffraction patterns of membrane and lipid systems typically contain about half the number of reflections (hence, twice the resolution value) of their x-ray counterparts.[1] The reconstructed x-ray and two neutron-scattering density profiles were therefore synthesized from $N$ and $N/2$ structure factors, respectively, for each resolution value ($d/N$) to be considered.

The set of six simultaneous equations and its five least-squares solutions were computed for each set of resynthesized profiles. The fractional error, $|\chi_{true} - \chi_{calc}|/|\chi_{true}|$, of each element, $\chi$, of the solution set is given in Table II as a function of resolution value.

As expected, the fractional errors tend to increase with increasing resolution value. Above 10-Å resolution value, the model calculation predicts that the reliability of some of the solutions begins to deteriorate. The uncertainties in the solutions are seen to be generally larger in the headgroup region (H), and are probably due to the fact that this region is made up of three components instead of two. We would therefore conclude that x-ray data from a membrane system with a resolution value $> 10$ Å, and companion neutron data with a resolution value $> 20$ Å, cannot be analyzed reliably by our method. Data with resolution values $\lesssim 10$ Å (x-ray)/20 Å (neutron), should have $\lesssim 10\%$ error in the computed solutions (see Table II). For the sake of completeness, the sensitivity of the calculations to errors in the accepted values of the x-ray and neutron-scattering densities (Table I) was examined using the same model membrane pair. The values of $\sigma^0$ and $\rho^0$ were varied over $\pm 10\%$. With one exception, errors in the calculated volume fractions were less than or of the same order as the introduced error: a $\pm$ 10% error in the scattering density values used for the protein produced an error of $\pm 0.21$ in the volume fraction, $g_w(C)$, of water in the cytoplasmic region of the model membrane pair.

Further studies with this model system demonstrate that only perfectly defined profiles (i.e., no smoothing of the profile and no resynthesis with a finite number of structure factors) will produce six correct solutions from the six equations. Errors in the data (e.g., the measured difference ratios) as small as 1% will produce gross errors in the solution set. Such small data errors, however, have a negligible effect on a set of five solutions calculated from the six simultaneous equations. We have, therefore, endeavored in our applications to limit the number of unknowns to five; this was possible without any loss of significant physical information in these systems.

We have applied the above theory to two ordered membrane-type systems for which x-ray and neutron-scattering profiles have been measured and which meet this 10-Å (x-ray)/20-Å (neutron) criterion: dipalmitoylphosphatidylcholine (DPC)-water multilayers and rabbit sciatic nerve myelin. Sets of simultaneous equations from

TABLE II
FRACTIONAL ERROR IN COMPUTED COMPONENT VOLUME FRACTIONS AS A FUNCTION OF RESOLUTION FOR MODEL MEMBRANE SYSTEM

| | Expected values | | | | |
|---|---|---|---|---|---|
| $B$ | $g_w(C)$ | $g_w(H)$ | $g_p(H)$ | $g_p(T)$ | |
| 1.000 | 0.770 | 0.500 | 0.340 | 0.560 | |
| | Fractional error* vs. resolution‡ | | | | |
| $B$ | $g_w(C)$ | $g_w(H)$ | $g_p(H)$ | $g_p(T)$ | *Resolution value (Å)* |
| 0.011 | 0.039 | 0.014 | 0.129 | 0.040 | 4.737 |
| 0.066 | 0.084 | 0.091 | 0.192 | 0.057 | 5.625 |
| 0.040 | 0.027 | 0.041 | 0.120 | 0.059 | 6.429 |
| 0.046 | 0.071 | 0.057 | 0.188 | 0.066 | 7.500 |
| 0.038 | 0.083 | 0.063 | 0.096 | 0.092 | 9.000 |
| 0.036 | 0.081 | 0.055 | 0.083 | 0.092 | 10.000 |
| 0.014 | 0.124 | 0.202 | 0.116 | 0.094 | 11.250 |
| 0.120 | 0.011 | 0.074 | 0.157 | 0.096 | 15.000 |
| 0.183 | 0.088 | 0.278 | 0.004 | 0.108 | 18.000 |
| 0.220 | 0.085 | 0.184 | 0.135 | 0.124 | 20.000 |
| 0.220 | 0.112 | 0.208 | 0.092 | 0.124 | 22.500 |
| 0.157 | 0.212 | 0.338 | 0.215 | 0.156 | 25.714 |
| 0.166 | 0.283 | 0.440 | 0.142 | 0.155 | 30.000 |
| 0.077 | 0.127 | 0.156 | 0.257 | 0.161 | 36.000 |
| 0.104 | 0.343 | 0.395 | 0.109 | 0.161 | 45.000 |

*Fractional error = $|\chi_{true} - \chi_{calculated}|/|\chi_{true}|$, $\chi = B, g_w(C), \ldots$
‡Resolution value of x-ray scattering density profile (= $d/N$, where $N$ is number of structure factors used in the synthesis of the profile); resolution value of neutron scattering density profile is twice that for the x-ray profile.

[1]For example, there are 18 orders of x-ray diffraction (3) vs. 7 orders of neutron diffraction for myelin (10); 16 orders of x-ray (20) vs. 6 orders of neutron (13) for rod outer segments; red cell membrane data (9) to 1/30 Å$^{-1}$ in x-ray vs. 1/45 Å$^{-1}$ in neutron diffraction patterns; and 11 orders of x-ray (21) vs. 8 orders of neutron (11) in DPC-water multilayers.

the x-ray and neutron-scattering profiles of the two systems were derived and solved as discussed above.

## APPLICATIONS

### Lipid Multilayers

The x-ray scattering density (electron density) profiles of L-$\alpha$-DPC-water multilayers were derived by Torbet and Wilkins (21) from 11 orders of diffraction (57.7-Å periodicity). Neutron-scattering profiles of this system were calculated (eight orders of a 57.7-Å periodicity) by Worcester (11). The scattering profiles are shown in Fig. 2. Both samples were prepared by evaporating the organic solvent from a lipid solution on a glass substrate and then hydrating the specimen by equilibration over a wet atmosphere of an inert gas at constant relative humidity. Since neither paper gave the structure factors used to synthesize the neutron or x-ray scattering density profiles, the difference ratios were measured directly from the published profiles. The value for the bulk lipid/water ratio (cf. Table III) for DPC-water multilayers at 57.7-Å spacing (25°C) was taken from a third source (22).

The three points used for calculation of the difference ratios (Eqs. 5–7) were the water layer ($x_i$), the methylene chain of the lipid ($x_j$), and the phospholipid headgroups ($x_k$). The water layer between phospholipid bilayers, designated "W" in Fig. 2, is identified with the midpoint between the lipid bilayers ($|x| = 28.8$ Å). Since the multilayers are being examined under conditions of partial dehydration, this region is allowed to be occupied by a volume fraction of water, $g_w$(W), which may be less than the volume fraction of bulk water (i.e., 1.0).

It has been demonstrated (24) in hydrated lecithin bilayers (with or without cholesterol) that the choline and the phosphoryl groups lie in a plane parallel to the bilayer surface, and therefore both of these groups were included in a calculation of the projected scattering densities of the headgroup. The phosphorylcholine group of the lipid headgroup region, at $|x| = 24$ Å, is observed to be clearly resolved from the glycerol moiety, at $|x| = 19$ Å, and the latter was therefore not included as part of the headgroup region. The scattering densities at the headgroup position ($|x| = 24$ Å) will be assumed to be composed of two components, a volume fraction $g_w$(H) of exchangeable water and $(1 - g_w[H])$ of phosphorylcholine groups with, of course, no exchangeable hydrogens. (It is assumed that, after equilibration, the ratio of $H_2O/D_2O$ in this region is the same as that in the saturated salt solution that produces the hydrating atmosphere for the multilayers.)

The paraffin tail of the lipid bilayer ($5 \leq |x| \leq 15$ Å) provides the third well-defined region for the calculation. This region (designated T) is tentatively allowed to be occupied by water [volume fraction, $g_w$(T)] and paraffin chains [volume fraction 1-$g_w$(T)]. (The center of the phospholipid hydrocarbon core, occupied by the terminal methyl groups, could equally well have been used in the calculation. Since the methylene region is constant over a significant portion of the profile, it was used for purposes of the calculation.) The calculated scattering densities for

TABLE III

PARAMETERS, COEFFICIENTS, AND SOLUTIONS TO SIMULTANEOUS EQUATIONS FOR DPC-WATER MULTILAYERS

A. Observed parameters

| Difference ratios | | | | Neutron-scattering density averages | | | |
|---|---|---|---|---|---|---|---|
| | | | | Profiles | | Chemical composition | |
| X-ray | Neutron | | | (*AU**) | | $10^{14}$ cm/Å$^3$ | |
| $R_0$ | $R_1$ (100% $H_2O$) | $R_2$ (100% $D_2O$) | $R_3$ ($D_2O$ – $H_2O$ 100%) | $\bar{\eta}_1$ | $\bar{\eta}_2$ | $\bar{\sigma}_1$ | $\bar{\sigma}_2$ |
| 0.033 | −0.233 | 1.296 | 1.980 | 5.0 | 13.5 | 0.108 | 0.853 |

B. Simultaneous equations

| | | | | | | | |
|---|---|---|---|---|---|---|---|
| 0.0 | 0.43 | −4.45 | 33.40 | | | | 29.38 |
| 0.0 | 3.94 | −3.57 | 6.09 | | $B$ | | 6.37 |
| 0.0 | −6.74 | 1.96 | 6.30 | × | $g_w(H)$ | = | 1.52 |
| 0.0 | −13.66 | −6.76 | 6.90 | | $g_w(T)$ | | 0.0 |
| 13.50 | 0.0 | 6.66 | 0.0 | | $g_w(W)$ | | 1.16 |
| 8.50 | 0.0 | 6.90 | 0.0 | | | | 0.75 |

C. Solutions by least squares

| $B$ | $g_w(H)$ | $g_w(T)$ | $g_w(W)$ |
|---|---|---|---|
| *0.11* | 0.47 | −0.05 | 0.86 |

L-$\alpha$-DPC-water multilayers made by partial hydration (25°C) from dried film. Lamellar repeat 57.7 Å. Lipid: weight fraction 0.89 (at $d$ = 57.7 Å, reference 22); specific volume 1.017 cm$^3$/g (reference 23); volume fraction 0.992.

*AU, arbitrary units.

each of the constituents in the three regions (W, H, and T) are listed in Table I.

The relative heights at the three points, W, H, and T, of the three profiles (Fig. 2), the relative volume fractions of lipid and water (Table III), and the calculated scattering densities of the constituents of the three regions of interest (Table I) have been substituted into Eqs. 5–7, 14, and 15. The six equations in four unknowns are presented in matrix form in Table III. As an example, we calculate one of the difference ratios, $R_1$, for this system. Using the calculated neutron density profile at 0% $D_2O$ (Fig. 2), the difference ratio of Eq. 6 is $R_1 = -0.233$. Calculating from Eq. 9 (using Table I)

$$\sigma_1(W) = -0.6\, g_w(W) + 0.00\,[1 - g_w(W)]$$

$$\sigma_1(H) = -0.6\, g_w(H) + 1.10\,[1 - g_w(H)]$$

$$\sigma_1(T) = -0.6\, g_w(T) - 0.31\,[1 - g_w(T)]$$

and substituting into Eq. 6 produces the second equation in Table III.

The set of six simultaneous equations derived from Eqs. 5–7, 14, and 15 are tabulated, with their least-squares solutions, in Table III. We find that the phosphorylcholine headgroup region is made up of 47% water by volume. This is equivalent to six water molecules per headgroup (using 30 Å$^3$ and 204 Å$^3$ for the respective volumes of a water molecule and a phosphorylcholine group [25]). This value is in good agreement with the value (5.7 water molecules/molecule egg lecithin) interpolated from the results of Small (25), taking the weight fraction of lipid to be 0.89 at $d$ = 57.7 Å from the work of Chapman et al.(22).

No water is present in the hydrophobic region of the bilayer (the small negative value is within the limits of error for the calculation). This result confirms what has long been suspected (25–27) but, until now, not experimentally demonstrated. Our conclusion is consistent with the measurements by Schatzberg (28) of the extremely low solubility of water in hexadecane (54 ppm by weight), a model compound for the palmitoyl paraffin chains that make up the hydrophobic core. This result is also in good agreement with permeability measurements and the corresponding solubility-diffusion model (29) for water permeation across lipid bilayers: the existence of water pores is excluded as a means of water transport across the bilayer (unless of course they are sufficiently dilute to go undetected by this method).

The x-ray scattering density of the terminal methyl group region ($x = 0$) can now be calculated. From Eq. 8, and using $g_w(H) = 0.47$ and $g_w(T) = 0.0$, we find that $\rho(H) = 11.3 \times 10^{-14}$ cm/Å$^3$ and $\rho(T) = 8.1 \times 10^{-14}$ cm/Å$^3$. These two values allow the calculated x-ray scattering density profile, $\zeta(x)$, to be put on an absolute scale. Using these two values to scale Fig. 2*a*, the scattering density at $x = 0$ corresponds to $5.37 \times 10^{-14}$ cm/Å$^3$, or 0.192 electrons/Å$^3$ (see note ‡, Table I). This is not too different from the value of 0.167 electrons/Å$^3$ given by Gulik-Krzywicki et al. (30).

The water layer between lipid bilayers contains a volume concentration of water ($g_w[C] = 0.86$), somewhat less than that for bulk water (which would be 1.0). This may reflect the presence of water in the form of a hydrate organized around the polar headgroups rather than as a bulk water layer. This has been suggested by Chapman et al. (22) as an explanation for the absence of a water-ice transition in the calorimetric analysis of DPC-water systems with up to 20% water.

## Myelin

The x-ray scattering density profile of rabbit sciatic nerve myelin was recalculated from the 18 structure factors determined by Caspar and Kirschner (3) and the associated neutron-scattering profiles (7 structure factors at 100% $D_2O$ and 6 at 65% $D_2O$) from Kirschner et al. (10). As can be inferred from the profiles (Fig. 3), the 180-Å unit cell is composed of a pair of lipid bilayerlike structures separated by two aqueous layers, the cytoplasmic ($x \simeq 0$Å) and the extracellular ($x \simeq 90$ Å) regions. The two aqueous regions are presumed to contain water and protein (with 20% of the hydrogens of protein assumed to be exchangeable [10]). The cytoplasmic region (designated C in Fig. 3) is one of the well-defined regions for calculation of the difference ratios; consideration of the extracellular region has been omitted because its observed scattering densities (x-ray and neutron) are quite similar to that of the cytoplasm. As in the previous model calculation, the scattering density of the cytoplasmic region is taken as the average over $0 \leq x < 10$ Å.

The cytoplasmic phospholipid headgroup (H) and the center of the hydrophobic core (T) of the bilayer are the two remaining well-defined regions ($x_k$ and $x_j$, respectively) chosen for calculating the difference ratios. These regions are defined by the corresponding peak ($x = 19$ Å) and trough ($x = 42$ Å) in the x-ray scattering density profile.

As in the case of DPC, the maximum in the phospholipid headgroup peak (H region) is taken to represent the phosphate ester group, omitting the glycerol moiety from consideration. The exchangeable hydrogen of cholesterol is also not included in the calculation of the neutron-scattering density of the headgroup, as the hydroxyl group of cholesterol has been shown to position itself near the glycerol group in lipid bilayers (16, 31). The probable presence of water (volume fraction, $g_w[H]$) and of protein (volume fraction, $g_p[H]$) in the headgroup region was allowed for in the calculation.

The 4.6-Å reflection seen in x-ray diffraction patterns of nerve myelin (which arises from the side-to-side packing of the phospholipid tails) is well oriented perpendicular to the lamellar reflections (32). From this, and other evidence, it has been concluded (33) that the long axes of the lipid hydrocarbon chains are aligned perpendicular to the

membrane plane, an effect that has been noted in other natural and artificial membranes containing cholesterol (33). The center of the lipid bilayer of myelin (T region) is therefore best represented by the scattering density of the terminal methyl groups rather than by that of the methylene chains of the phospholipid.

The volume fraction $g_p(T)$ represents protein potentially located at the center of the lipid core. Because of the restriction that the number of unknowns be less than the number of equations (providing the solution set sufficient freedom to compensate for the finite resolution of the data), it is assumed that no water is present at the center of the lipid hydrocarbon. Such an assumption is consistent with the results derived from the DPC-water system. As we will show, hydrogens of the lipid core protein do not seem to undergo H → D exchange, further supporting this assumption.

Four difference ratios were constructed from the observed x-ray and neutron-scattering profiles, substituting the C, T, and H regions (Fig. 3) for $x_i$, $x_j$ and $x_k$, respectively, in Eqs. 5–7. The bulk volume fractions of lipid, protein, and water (Table IV) used to construct the fifth and sixth equations (Eqs. 14 and 15) were taken from references 3 and 10. Solutions were calculated for two cases: (*a*) none of the protein confined to the hydrocarbon tail region (T) exchanges H for D and (*b*) all exchangeable hydrogens of this protein are exchanged. The six simultaneous equations (in matrix form) for the first case, and the solutions for both cases *a* and *b* are given in Table IV.

The set of simultaneous linear equations (Table IV) was solved using the least-squares method described above. Only the case which assumes that protein in the hydrocarbon tail region cannot exchange H for D (*a*) produces meaningful results. This result is strong evidence that almost all of the protein (50%) buried in the lipid core is inaccessible to the aqueous milieu. (The fact that this protein does not undergo H → D exchange with the aqueous regions supports the earlier assumption that no water is present in the hydrocarbon tail region.)

The headgroup region is hydrated with about the same amount of water [$g_w(H) = 0.53$] as in the DPC-water system [$g_w(H) = 0.47$]. This region also contains slightly more protein by volume [$g_p(H) = 0.29$] than do the aqueous (extracellular and cytoplasmic) regions, which contain only 18% protein by volume [$1 - g_w(C) = 0.18$].

The overall protein concentration appears to follow a

TABLE IV
PARAMETERS, COEFFICIENTS, AND SOLUTIONS TO SIMULTANEOUS EQUATIONS FOR RABBIT SCIATIC NERVE MYELIN

A. Observed parameters

| Difference ratios | | | | Neutron-scattering density averages | | | |
|---|---|---|---|---|---|---|---|
| X-ray | Neutron | | | Profiles (AU)* | | Chemical composition ($10^{14}$ cm/Å$^3$) | |
| $R_0$ | $R_1$ (65% $D_2O$) | $R_2$ (100% $D_2O$) | $R_3$ (100% $D_2O$ − 65% $D_2O$) | $\bar{\eta}_1$ | $\bar{\eta}_2$ | $\bar{\sigma}_1$ | $\bar{\sigma}_2$ |
| 0.617 | 1.235 | 1.287 | 1.413 | 0.74 | 1.06 | 2.13 | 3.17 |

B. Simultaneous equations

| | | | | | | | |
|---|---|---|---|---|---|---|---|
| 0.0 | 0.94 | −0.803 | −0.222 | 1.010 | | | 0.784 |
| 0.0 | 1.100 | −3.186 | −1.828 | 0.646 | | | −0.970 |
| 0.0 | 3.000 | −6.049 | −2.188 | 0.789 | | | −0.997 |
| 0.0 | 1.900 | −2.996 | −0.311 | 0.0 | × | = | −0.104 |
| 1.060 | 0.0 | 0.0 | 0.0 | 0.275 | | | 0.414 |
| 0.320 | 0.0 | 0.0 | 0.0 | 0.0 | | | 0.109 |

$$\begin{matrix} B \\ g_w(C) \\ g_w(H) \\ g_p(H) \\ g_p(T) \end{matrix}$$

C. Solutions by least squares

| | $B$ | $g_w(C)$ | $g_w(H)$ | $g_p(H)$ | $g_p(T)$ |
|---|---|---|---|---|---|
| (*a*) No exchangeable hydrogens in lipid hydrocarbon | 0.27 | 0.82 | 0.53 | 0.29 | 0.50 |
| (*b*) Exchangeable hydrogens (from protein) in lipid hydrocarbon | 0.31 | 1.35 | 0.93 | −0.16 | 0.22 |
| (*c*) Calculated using scattering densities for hydrophobic and hydrophilic protein residues | 0.24 | 0.70 | 0.45 | 0.35 | 0.66 |

Rabbit sciatic nerve myelin bathed in Ringer's solution. Lamellar periodicity 180 Å. Volume fractions: water − 0.42 (as measured by dimethyl sulfoxide dehydration [34], at a lamellar periodicity of $d$ = 180 Å; total water volume ≃ $[d - 105 \text{ Å}]/d = 0.425$], lipid − 0.49, and protein − 0.09. Protein constitutes ~0.18 of the dry weight of rabbit sciatic nerve myelin (35). This corresponds to a (dry) volume fraction of 0.14 (using $\bar{v}_p = 0.7$ and $\bar{v}_\ell = 0.98$ as the partial specific volumes of protein and lipid; cf. Eq. 11 of text).
*AU, arbitrary units.

general distribution of decreasing concentration outward from the lipid core, beginning with a 50% protein concentration at the center of the lipid core, ~30% protein at the headgroup, and 20% in the extralipid regions. Kirschner et al. (10) estimated, using contrast matching arguments, that there is 9–14% protein in the aqueous regions of rabbit sciatic nerve myelin, and that the hydrocarbon region contains, on the average, only 4–9% protein. Although this latter value is not easily reconciled with the 50% volume fraction we calculate at the center of the hydrocarbon core, the discrepancy may be due, at least in part, to the assumptions and approximations inherent in their calculation based on contrast matching. In addition, biochemical studies (36) show that 70% of the major peripheral nerve protein ($P_0$), which comprises 50% or more of the total protein (37), is hydrophobic and trypsin inaccessible, which is consistent with our prediction.

It should be noted that the above results do not change drastically if we assume that the center of the bilayer contains an overlap of lipid $CH_3$ and $CH_2$ groups. For example, for 50% $CH_3$ plus 50% $CH_2$ (which we believe to be an extreme case) we calculate: $g_w(C) = 0.85$, $g_w(H) = 0.55$, $g_p(H) = 0.24$, and $g_p(T) = 0.35$. Except for the last value, the other volume fractions are essentially the same as those previously obtained (see Table IV). The value for $g_p(T)$ shows that the estimate of protein in the tail region could be diminished somewhat from 50% if $CH_2$ groups overlap $CH_3$ in this region.

It could be argued that polar and hydrophobic portions of the membrane proteins could be at least partially partitioned between the two respective regions of the membrane lipid. This would lower the (x-ray and neutron) scattering densities of protein at the hydrocarbon tail (T) region. We have repeated the volume fraction calculations with the extreme assumption that the membrane protein is completely segregated, viz., the hydrocarbon tail region contains only protein with all of the hydrophobic amino acids. Their respective scattering densities were calculated using the known amino acid compositions of the major proteins of rabbit sciatic nerve myelin (35), and their corrected calculated specific volumes (38). As seen in Table IV (*C*), the calculated volume fractions are not too different from those obtained from average protein scattering densities. The largest difference, seen between the two volume fractions of protein at the hydrocarbon core, $g_p(T)$, is 0.16.

## CONCLUSIONS

The method presented here combines both x-ray and neutron-scattering density profiles to obtain a profile of the biochemical constituents of the membrane. Although we have confined our analysis to the lipid headgroup, the hydrocarbon tail, and the extralipid regions, it is possible to calculate component volume fractions for other regions: this would only require knowledge of the specific component scattering densities at these points. As we have shown, the results are more accurate the better the resolution in the scattering data.

For the DPC multilayers, we have confirmed and quantified three hypotheses previously based on model and water permeability (rather than structural) studies: (*a*) the lipid hydrocarbon core contains no measurable ($-5 \pm 10\%$) water, either in the form of a pore through the bilayer or trapped within the interior (28, 29); (*b*) the headgroup region is highly hydrated (~47% by volume) (25); and (*c*) the water in the extralipid regions of lipid-water multilayers is not present as liquid water [i.e., with $g_w(W) = 1.0$] but is more likely complexed with the phospholipid headgroups (22).

Our calculations for the myelin membrane show that such hydration of lipid headgroups is also present here. In addition we find that the extracellular and cytoplasmic regions contain ~20% protein by volume. (Kirschner et al. [10] estimated 9–14% protein content for these regions.) We have, for the first time in a native membrane, also determined the protein compositions in the lipid headgroup and hydrocarbon tail regions, ~30% by volume in the former and ~50% by volume in the latter regions. Furthermore, we find that most of the protein in the lipid core does not undergo H → D exchange, presumably indicating that it is inaccessible to the aqueous milieu. The above volume fractions, together with the known average specific volume of globular proteins, suggests that this protein cannot extend over much more than 5–10 Å centered at the tail region. Possible errors due to (*a*) truncation of diffraction data, (*b*) errors in the accepted values of component scattering densities, and (*c*) the partition of hydrophobic and hydrophilic protein segments were examined. These do not produce errors in the calculated volume fractions of $> \pm 0.2$ in any component, with likely errors being closer to $\pm 0.1$.

We have not extended this analysis to other membranes (e.g., rod outer segments [4–6, 12, 13] and the red cell membrane [9]) because complementary x-ray and neutron diffraction data on these systems do not satisfy our resolution criterion (a resolution value $\leqq$ ~10 Å in x ray and 20 Å in neutron). It is quite clear, however, that improved resolution in the data for such systems will make it feasible to obtain biochemical profiles on these membranes.

This research was supported by National Institutes of Health grant HL18737.

*Received for publication 15 May 1980.*

## REFERENCES

1. Finean, J. B. 1969. Biophysical contributions to membrane structure. *Q. Rev. Biophys.* 2:1–23.
2. Worthington, C. R., and G. I. King. 1971. Electron density profiles of nerve myelin. *Nature (Lond.).* 234:143–145.
3. Caspar, D. L. D., and D. A. Kirschner. 1971. Myelin membrane structure at 10 Å resolution. *Nat. New Biol.* 231:46–52.
4. Blasie, J. K., M. M. Dewey, A. E. Blaurock, and C. R. Worthington. 1965. Electron microscopy and low angle x-ray diffraction studies

on outer segment membranes from the retina of a frog. *J. Mol. Biol.* 14:143–152.
5. Gras, W. J., and C. R. Worthington. 1969. X-ray analysis of retinal photoreceptors. *Proc. Nat. Acad. Sci. U.S.A.* 63:233–238.
6. Blaurock, A. E., and M. H. F. Wilkins. 1969. Structure of frog photoreceptor membranes. *Nature (Lond.).* 223:906–909.
7. Stamatoff, J. B., S. Krimm, and N. R. Harvie. 1975. X-ray diffraction studies of human erythrocyte membrane stucture. *Proc. Natl. Acad. Sci. U.S.A.* 72:531–534.
8. Pape, E. H., K. Klott, and W. Kreutz. 1977. The determination of the electron density profile of the human erythrocyte ghost membrane by small-angle scattering x-ray diffraction. *Biophys. J.* 19:141–161.
9. McCaughan L., and S. Krimm. 1980. X-ray and neutron scattering density profiles of the intact human red blood cell membrane. *Science Wash. D.C.* 207:1481–1483.
10. Kirschner, D. A., D. L. D. Caspar, B. P. Schoenborn, and A. C. Nunes. 1976. Neutron diffraction studies of nerve myelin. In Neutron Scattering for the Analysis of Biological Structures. *Brookhaven Symp. Biol.* 27: III-68–76.
11. Worcester, D. L. 1975. Neutron beam studies of biological membranes and membrane components, In Biological Membranes. D. Chapman and D. H. F. Wallach, editors, Academic Press, Inc., Ltd., London. 3:1–46.
12. Yeager, M. J. 1976. Neutron diffraction analysis of the structure of retinal photoreceptor membranes and rhodopsin, In Neutron Scattering for the Analysis of Biological Structures. *Brookhaven Symp. Biol.* 27:III-3–23.
13. Chabre, M., H. Saibil, and D. L. Worcester. 1976. Neutron diffraction studies of oriented retinal rods. In Neutron Scattering for the Analysis of Biological Structures. *Brookhaven Symp. Biol.* 27:III-77–85.
14. Bacon, G. E. 1962. Neutron Diffraction. Clarendon Press, Oxford. 368 pp.
15. O'Brien, J. S., E. L. Sampson, and M. B. Stern. 1967. Lipid composition of myelin from the peripheral nervous system. *J. Neurochem.* 14:357–365.
16. Worcester, D. L., and N. P. Franks. 1976. Structural analysis of hydrated egg lecithin and cholesterol bilayers. *J. Mol. Biol.* 100:359–378.
17. Faddeev, D. K., and V. N. Faddeeva. 1963. Computational Methods of Linear Algebra. W. H. Freeman & Co., San Francisco, Calif. Chap. 11. 621 pp.
18. Lawson, C. L., and R. J. Hanson. 1974. Solving Least Squares Problems. Prentice-Hall, Inc., Englewood Cliffs, N. J. 340 pp.
19. The International Mathematical and Statistical Libraries, Inc., Reference Manual. 1979. Houston, Tex. 7th edition. 370 pp.
20. Schwartz, S., J. E. Cain, E. A. Dratz, and J. K. Blasie. 1975. An analysis of lamellar x-ray diffraction from disordered membrane multilayers with application to data from retinal rod outer segments. *Biophys. J.* 15:1201–1233.
21. Torbet, J., and M. H. F. Wilkins. 1976. X-ray diffraction studies of lecithin bilayers. *J. Theor. Biol.* 62:447–458.
22. Chapman, D., R. M. Williams, and B. D. Ladbrooke. 1967. Physical studies of phospholipids. *Chem. Phys. Lipids.* 1:445–475.
23. Reiss-Husson, F. 1967. Structure des phases liquide-cristallines de différents phospholipides, monoglycérides, sphingolipides, anhydres ou en presence d'eau. *J. Mol. Biol.* 25:363–382.
24. Worcester, D. L. 1976. Neutron diffraction studies of biological membranes and membrane components. In Neutron Scattering for the Analysis of Biological Structures. *Brookhaven Symp. Biol.* 27:III-37–57.
25. Small, D. M. 1967. Phase equilibria and structure of dry and hydrated egg lecithin. *J. Lipid Res.* 8:551–557.
26. Leathes, J. B. 1925. Role of fats in vital phenomena. *Lancet* I:1019.
27. Tanford, C. 1978. The hydrophobic effect and the organization of living matter. *Science (Wash. D.C.).* 200:1012–1018.
28. Schatzberg, P. 1963. Solubilities of water in several normal alkanes from $C_7$ to $C_{16}$. *J. Phys. Chem.* 67:776–779.
29. Price, H. D., and T. E. Thompson. 1969. Properties of liquid bilayer membranes separating two aqueous phases: temperature dependence of water permeability. *J. Mol. Biol.* 41:443–457.
30. Gulik-Krzywicki, T., E. Rivas, and V. Luzzati. 1967. Structure et polymorphisme des lipides: études par diffraction des rayons du système formé de lipides de mitochondries de loeur de boeuf et d'eau. *J. Mol. Biol.* 27:303–322.
31. Blasie, J. K., G. Zaccai, and B. Schoenborn 1975. High-resolution neutron diffraction studies of lecithin and lecithin-cholesterol lipid bilayers. *Biophys. J.* 15:99 (Abstr.).
32. Schmitt, F. O., R. S. Bear, and G. L. Clark. 1935. X-ray diffraction studies on nerve. *Radiology* 25:131–151.
33. Levine, Y. K. 1973. X-ray diffraction studies of membranes. *Prog. Surf. Membr. Sci.* 3:279–352.
34. Kirschner, D. A., and D. L. D. Caspar. 1975. Myelin structure transformed by dimethyl sulfoxide. *Proc. Natl. Acad. Sci. U.S.A.* 72:3513–3517.
35. Greenfield, S., S. Brostoff, E. H. Eylar, and P. Morell. 1973. Protein composition of myelin of the peripheral nervous system. *J. Neurochem.* 20:1207–1216.
36. Roomi, M. W., and E. H. Eylar. 1978. Isolation of a product from the trypsin-digested glycoprotein of sciatic nerve myelin. *Biochim. Biophys. Acta.* 536:122–133.
37. Roomi, M. W., A. Ishaque, N. R. Khan, and E. H. Eylar. 1978. The PO protein. The major glycoprotein of peripheral nerve myelin. *Biochim. Biophys. Acta.* 536:112–121.
38. Cohen, E. J., and Edsall, J. T. 1943. Proteins, Amino Acids and Peptides. Reinhold Publishing Corp., New York. 370–375.